Robust Speed Control of Electrical Drives With Reduced Ripple Using Adaptive Switching High-Order Extended State Observer

Shanfeng Zhu, Wenxin Huang, *Member, IEEE*, Yajun Zhao, Xiaogang Lin, *Member, IEEE*, Dingfeng Dong, Wen Jiang, Yong Zhao, and Xu Wu

***Abstract*—Active disturbance rejection control using extended state observer (ESO) is less dependent on the knowledge of the system. It has proved to be an excellent scheme for speed control of electrical drives. However, for time-varying disturbance, the observation precision of conventional ESO is undesired, which limits the speed tracking accuracy. Accordingly, this article proposes an enhanced speed controller for electrical drives based on adaptive switching high-order ESO (ASHESO). First, the critical parameters affecting the steady-state performance of ASHESO are determined according to frequency analytical results. Then, optimized observer gain is obtained by modifying a part of pole locations, which weakens the influence of noise on estimated state. Finally, an adaptive switching gain mechanism is proposed according to the closed-loop tracking error and the swiftness of dynamic response is maintained. The proposed speed controller has achieved high estimation accuracy for disturbance and strong immunity to measurement noise. The feasibility and effectiveness of the strategy is verified on a laboratory permanent magnet synchronous motor (PMSM) drive system.**

***Index Terms*—Active disturbance rejection control (ADRC), electrical drives, extended state observer (ESO), speed control.**

I. Introduction

ELECTRICAL drive system that includes rotary motors is widely used in industrial applications, and its application is developing rapidly [1], [2]. Speed control is a common operating mode of electrical drive system. Under this mode, the outer speed loop provides the reference signal for the inner current loop. Therefore, it has dominant impacts on the performance of the overall drive system. Traditional control methods based on linear feedback, like proportional–integral (PI) control, is widely applied in speed loop. It has advantages of simple structure and high reliability [3]. Nevertheless, the periodic and nonperiodic disturbances/uncertainties, such as sampling errors, flux harmonics, cogging torques, and load variations are commonly existent in electrical drive system. It is difficult for PI control to mitigate these disturbances efficiently [4]–[6].

To cope with the periodic disturbances, iterative learning control, repetitive control, and proportional resonant control [7]–[10] are applied to speed control of electrical drives. However, since the above-mentioned methods can only produce large open-loop gains on specific frequencies, they are unable to rapidly suppress the nonperiodic disturbance, resulting in unsatisfactory dynamic performance. The methods based on disturbance estimation are another kind of scheme to improve speed performance, including disturbance observer [11], unknown input observer [12], uncertainty and disturbance estimator [13], sliding mode observer [14], and extended state observer (ESO) [15], [16]. By observing disturbance and compensating it to the control signal in real time, they can quickly attenuate the effect of disturbance on the system. Among these observers, ESO requires the least amount of plant information. It regards the internal uncertainties, external disturbances and unmodeled dynamics as total disturbance and estimates it with state variables simultaneously. For its superior properties, the composite control framework based on ESO, called active disturbance rejection control (ADRC), has been widely investigated in recent years [17]–[22].

Despite the wide application of ADRC in industry, the performance of ESO is still limited with regard to torque ripple estimation, because it is unable to ensure the asymptotic estimation of time-varying disturbance [23]. In order to reduce the estimation error of time-varying disturbance, some novel structures of ESO are proposed by scholars. One type is called resonant extended state observer (RESO), which divides the resonant part from the composition of total disturbance. Real-time and high-precision acquisition of disturbance frequency is vital for such method [24], [25]. Therefore, RESO is sensitive to the significant frequency variation. The other type is high-order extended state observer (HESO). By increasing the number of the extended states, the asymptotic convergence of the high-order term in the polynomial form of disturbance can be realized and then the estimation accuracy of the time-varying disturbance will be improved [23], [26]. Compared with RESO, the design of HESO needs less information about disturbance, therefore, it is not sensitive to the variation of disturbance frequency. In addition,

Manuscript received March 27, 2021; revised June 26, 2021; accepted August 9, 2021. Date of publication August 18, 2021; date of current version October 15, 2021. This work was supported by the National Natural Science Foundation of China under Grant 51777096. Recommended for publication by Associate Editor G. De Donato. *(Corresponding author: Wenxin Huang.)*

The authors are with the Jiangsu Key Laboratory of New Energy Generation and Power Conversion, College of Automation Engineering, Nanjing University of Aeronautics and Astronautics, Nanjing 210016, China (e-mail: zsf_nuaa2@163.com; huangwx@nuaa.edu.cn; zhaoyajun008@163.com; xg_lin_nuaa@126.com; dong_dingfeng@126.com; nuaa_jw@163.com; zhaoyong1105@nuaa.edu.cn; wuxu0922@163.com).

Color versions of one or more figures in this article are available at https://doi.org/10.1109/TPEL.2021.3105263.

Digital Object Identifier 10.1109/TPEL.2021.3105263

HESO does not require multiple harmonic models and it is simpler for implementation. The disadvantage of HESO is its weak ability to noise suppression, which limits the control accuracy of observer. If the noise sensitivity of HESO is lessened, the capability of rejecting disturbance can be further improved.

The influence of measurement noise on HESO is serious under the conventional observer gain [27]. Scholars have made following enhancements on ESO to attenuate the effects of noise. In [28], an additional integral state variable is introduced to expand the model of the plant, which partially decouples noise and observer gain. Improvement of the smoothness of observed value was presented in this article. However, the integration will bring phase delay to the observed states and affect the compensation accuracy. In [29], the gain tuning law using Kalman filter type algorithm was proposed to balance noise suppression and disturbance rejection performance. It provided the linear minimum variance estimation for total disturbance under some conditions. Nonetheless, the complexity of the algorithm increased a lot during the calculation of the observer gain. The cascaded structure of ESO was proposed in [30]. The signal is filtered by the previous level of ESO and, thus, the next level of ESO is affected by noise to a smaller extent. However, the delay introduced by the previous ESOs will diminish the tracking rate of the signal. To conclude, the abovementioned techniques had generally increased ESOs ability of noise attenuation, but the drawback of reduced signal convergence rate and lower estimation accuracy will deteriorate the speed performance.

In this article, an enhanced speed controller based on adaptive switching high-order ESO (ASHESO) is proposed. A new set of optimized gain and adaptive switching gain mechanism are obtained by ASHESO. Compared with [29], the optimized gain retains the bandwidth item and the tuning work is greatly simplified. Moreover, it merits better steady-state performance than traditional observer proposed in [25] and [27] for less sensitivity to noise and enhanced estimation accuracy. Additionally, ASHESO switches the gain according to the tracking error to keep the rapid tracking performance. Therefore, the convergent rate of estimates is faster than the ESO structures proposed in [28] and [30].

The rest of this article is organized as follows: Section II introduces the speed loop control structure based on HESO. Section III presents proposed ASHESO including the noise suppression method and adaptive switching gain scheme. Experiments are designed to verify the proposed method in Section IV. Finally, Section V concludes this article.

II. ADRC-Based Speed Loop Controller Design

A. Modeling of Mechanical Dynamics for Electric Drive

It is well known that the mechanical dynamics for electric motor drive can be described by

$$J\dot{\omega}_m + B\omega_m = K_t i_q - T_d, \quad T_d = T_L + T_R \tag{1}$$

where ω_m is the angular speed and K_t is the torque constant. i_q represents the q-axis current in synchronous frame. J and B are the total inertia and the viscous friction coefficient. T_d is the disturbance torque including load torque T_L and torque ripple T_R.

The above-mentioned equation can be reformulated in the canonical form as follows:

$$\begin{aligned}\dot{\omega}_m &= \frac{K_t}{J} i_q - \frac{B}{J}\omega_m - \frac{T_d}{J} = b i_q - \frac{B}{J}\omega_m - \frac{T_L}{J} - \frac{T_R}{J} \\ &= b_0 i_q^{ref} + f \end{aligned} \tag{2}$$

where i_q^{ref} is q-axis current reference and $b = K_t/J$ represents the control gain. It is reasonable to set the estimated gain as $b_0 = K_{tn}/J_n$ using the nominal value of the plant. The total disturbance f is defined by

$$\begin{aligned} f = &\left[(b - b_0) i_q^{ref} + b(i_q - i_q^{ref}) - \frac{B}{J}\omega_m - \frac{T_L}{J}\right] \\ &- \frac{T_R}{J} = f_0 + f_R \end{aligned} \tag{3}$$

where $f_0 = (b - b_0) i_q^{ref} + b(i_q - i_q^{ref}) - B\omega_m/J - T_L/J$ signifies slow-varying disturbances. (b-b_0)a i_q^{ref} is the error caused by parameter variations. $b(i_q$-$i_q^{ref})$ is tracking error of q-axis current. $B\omega_m/J$ is the disturbance caused by the friction force and T_L/J is the load torque disturbance. f_R = -T_R/J represents fast-varying torque ripple disturbance, which arises from nonideal factors like sensor scaling/offset error, dead time effect of inverter, and nonsinusoidal flux distribution of motor.

B. Controller Design Based on High-Order ESO

We set torque current reference i_q^{ref} as control signal u, speed reference w_m^{ref} as reference signal r, speed ω_m as output signal y. Define state variable as $x_1 = \omega_m$ and $x_2 = f$, where f is the extended state variable.

Consider the dynamic system of (2), if the nth rate of change of the uncertainty is negligible, then, the extended order system for (2) by considering n additional states can be written as

$$\begin{bmatrix} \dot{x}_1 \\ \dot{x}_2 \\ \vdots \\ \dot{x}_n \\ \dot{x}_{n+1} \end{bmatrix} = \begin{bmatrix} 0 & 1 & 0 & \cdots & 0 \\ 0 & 0 & 1 & 0 & 0 \\ \vdots & \vdots & \vdots & \ddots & \vdots \\ 0 & 0 & 0 & 0 & 1 \\ 0 & 0 & 0 & 0 & 0 \end{bmatrix} \begin{bmatrix} x_1 \\ x_2 \\ \vdots \\ x_n \\ x_{n+1} \end{bmatrix} + \begin{bmatrix} b_0 \\ 0 \\ \vdots \\ 0 \\ 0 \end{bmatrix} u + \begin{bmatrix} 0 \\ 0 \\ \vdots \\ 0 \\ 1 \end{bmatrix} f^{(n)} \tag{4}$$

where x_i (i = 1, 2, …, n+1) stands for state variable and $f^{(n)}$ represents n order derivative of the variable f.

As the general form of ESO, the linear HESO is expressed as

$$\begin{bmatrix} \dot{z}_1 \\ \dot{z}_2 \\ \vdots \\ \dot{z}_n \\ \dot{z}_{n+1} \end{bmatrix} = \begin{bmatrix} 0 & 1 & 0 & \cdots & 0 \\ 0 & 0 & 1 & 0 & 0 \\ \vdots & \vdots & \vdots & \ddots & \vdots \\ 0 & 0 & 0 & 0 & 1 \\ 0 & 0 & 0 & 0 & 0 \end{bmatrix} \begin{bmatrix} z_1 \\ z_2 \\ \vdots \\ z_n \\ z_{n+1} \end{bmatrix} + \begin{bmatrix} b_0 \\ 0 \\ \vdots \\ 0 \\ 0 \end{bmatrix} u + \begin{bmatrix} \beta_1 \\ \beta_2 \\ \vdots \\ \beta_n \\ \beta_{n+1} \end{bmatrix} [x_1 - z_1] \tag{5}$$

where z_i (i = 1, 2, …, n+1) is the estimate of state variable x_i, n is the extension order, and β_i (i = 1, 2, …, n+1) is the observer gain. Specifically, (5) is equivalent to conventional ESO when

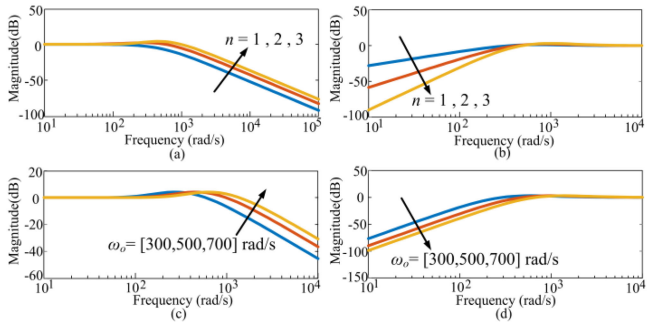

Fig. 1. Bode diagram of $G_z(s)$ and $G_e(s)$. (a) Different orders for $G_z(s)$. (b) Different orders for $G_e(s)$. (c) Different bandwidths for $G_z(s)$. (d) Different bandwidths for $G_e(s)$.

$n = 1$. As the observer converges, the estimate z_i approximates to the state variable x_i.

The observer error dynamics could be derived by subtracting (5) from (4)

$$\begin{bmatrix} \dot{e}_1 \\ \dot{e}_2 \\ \vdots \\ \dot{e}_n \\ \dot{e}_{n+1} \end{bmatrix} = \begin{bmatrix} -\beta_1 & 1 & 0 & \cdots & 0 \\ -\beta_2 & 0 & 1 & 0 & 0 \\ \vdots & \vdots & \vdots & \ddots & \vdots \\ -\beta_n & 0 & 0 & 0 & 1 \\ -\beta_{n+1} & 0 & 0 & 0 & 0 \end{bmatrix} \begin{bmatrix} e_1 \\ e_2 \\ \vdots \\ e_n \\ e_{n+1} \end{bmatrix} + \begin{bmatrix} 0 \\ 0 \\ \vdots \\ 0 \\ 1 \end{bmatrix} f^{(n)}. \quad (6)$$

If the bandwidth tuning method [24] is adopted, the closed-loop poles of the observer will be placed at the same position $-\omega_o$ and the gain coefficient will satisfy

$$\beta_i = \frac{(n+1)!}{i!(n+1-i)!}\omega_o^i, \quad i = 1,\ 2,\ \ldots,\ n+1 \quad (7)$$

and the characteristic polynomial is

$$D(s) = s^{n+1} + \beta_1 s^n + \beta_2 s^{n-1} + \cdots + \beta_{n+1} = (s+\omega_o)^{n+1}. \quad (8)$$

The transfer function of HESO from the observed value z_2 to the total disturbance f is denoted as follows:

$$G_z(s) = \frac{(s+\omega_o)^{n+1} - s^{n+1} - \beta_1 s^n}{(s+\omega_o)^{n+1}}. \quad (9)$$

The disturbance estimation error becomes

$$G_e(s) = 1 - G_z(s) = \frac{s^{n+1} + \beta_1 s^n}{(s+\omega_o)^{n+1}}. \quad (10)$$

To obtain the ideal step tracking response, the control law of loop is designed as

$$i_q^{ref} = \frac{k_p(r-y) - z_2}{b_0} = \frac{k_p(\omega_m^{ref} - \omega_m) - z_2}{b_o}. \quad (11)$$

If the total disturbance can be accurately estimated and compensated, the original plant is reduced to a pure integrator. Then, the closed-loop transfer function can be approximated as

$$\varphi(s) \approx \frac{k_p/s}{1 + k_p/s} = \frac{k_p}{s + k_p} \quad (12)$$

where $k_p \approx \omega_c$ represents the bandwidth of closed loop.

Fig. 1 plots the frequency characteristics of $G_z(s)$ and $G_e(s)$ of HESO. Fig. 1(a) and (b) shows the characteristics of $G_z(s)$ and $G_e(s)$ with different orders when bandwidth is $\omega_o = 500$ rad/s. Fig. 1(c) and (d) shows the characteristics of $G_z(s)$ and $G_e(s)$ with different bandwidths and the same order $n = 3$. It can be seen that when the order increases, the observed value is more sensitive to measurement noise but disturbance rejection ability is superior. Moreover, the disturbance rejection ability of HESO increases with the increase of bandwidth, but it is more sensitive to noise. Therefore, with the increase of order and bandwidth, the disturbance rejection ability of HESO is enhanced, but the robustness to noise is attenuated.

TABLE I
RISING TIME OF HESO FOR STEP DISTURBANCE ESTIMATION

Order	$G_z(s)$	Rising time T_r/s[31]
n=1	$\frac{\omega_o^2}{(s+\omega_o)^2}$	$\frac{3.4}{\omega_o}$
n=2	$\frac{3\omega_o^2 s + \omega_o^3}{(s+\omega_o)^3}$	$\frac{\sqrt{5}+1}{2\omega_o}$
n=3	$\frac{6\omega_o^2 s^2 + 4\omega_o^3 s + \omega_o^4}{(s+\omega_o)^4}$	$\frac{1}{\omega_o}$

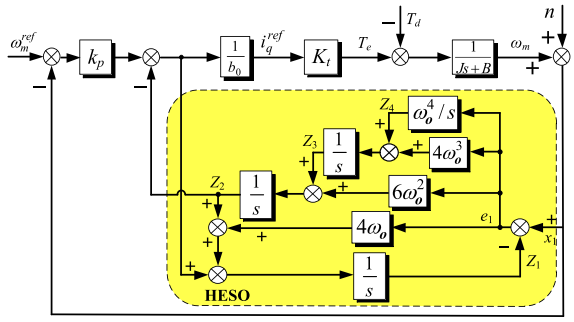

Fig. 2. Block diagram of speed control loop based on fourth-order HESO.

The time domain response of HESO with different order is given in Table I. It can be seen that increasing the bandwidth can reduce the rising time for HESO to track the step disturbance. In addition, the higher order gives rise to the faster tracking rate of HESO. Hence, increasing the order and bandwidth of HESO is favorable to swiftness of dynamic response but adverse to noise immunity.

For the sake of balance between the performance and complexity, we select fourth-order HESO, with three extended states, to observe the states and lumped disturbance in speed control loop. Fig. 2 is the control block diagram of speed loop based on fourth-order HESO. The whole system adopts the double-loop structure. PI regulator is used for current control and the inner loop is equivalent to unity for simplicity. The proportional regulator is used for outer loop control, added by feed-forward of the estimated disturbance by HESO to formulate the torque current reference.

III. OPTIMIZATION AND ADAPTIVE TUNING FOR ASHESO

According to the analysis in Section II, there are two main problems for conventional HESO: First, steady-state performance is limited under the conventional bandwidth tuning method, as the tradeoff exists between the disturbance rejection and noise immunity. Second, the presence of noise also forces the restriction on the convergence rate of the states. For the purpose of solving the abovementioned problems, an enhanced

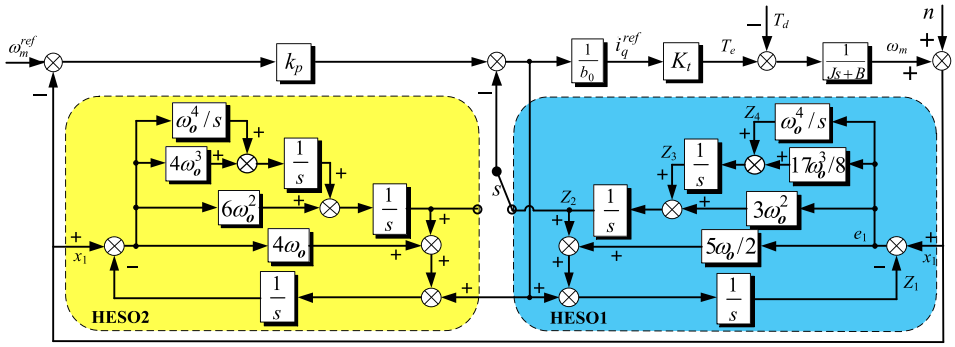

Fig. 3. Block diagram of speed control loop based on ASHESO.

speed controller based on ASHESO is proposed in this article. In Section III-A, the optimized observer gain is proposed to solve the first problem. In Section III-B, an adaptive switching gain mechanism is put forward to solve the second problem.

The block diagram of proposed controller is presented in Fig. 3. ASHESO adopts HESO1 during the steady state for noise reduction. It will adaptively switch to HESO2 during the transient state to achieve good dynamic performance.

A. Parameter Optimization of ASHESO Design

As mentioned previously, HESO has better disturbance estimation abilities but higher sensitivity to measurement noise. This part attempts to analyze parameters' impact on steady-state performance and optimize the observer with improved disturbance rejection and noise immunity.

The transfer function between estimated disturbance z_2 and total disturbance f for fourth-order HESO is shown as follows:

$$G_z(s) = \frac{\beta_2 s^2 + \beta_3 s + \beta_4}{s^4 + \beta_1 s^3 + \beta_2 s^2 + \beta_3 s + \beta_4}. \tag{13}$$

Considering the influence of measurement noise, the control law is formulated by

$$u = \frac{k_p(r - y - n) - z_2}{b_0}. \tag{14}$$

The observed disturbance satisfies the following formula:

$$z_2 = G_z(s)(s(y+n) - b_0 u) = G_z(s)(f + sn). \tag{15}$$

Thus, the following characteristics could be derived:

$$\begin{cases} G_r(s) = \frac{y(s)}{r(s)} = \frac{k_p}{k_p+s} \\ G_f(s) = \frac{y(s)}{f(s)} = \frac{1-G_z(s)}{k_p+s} \\ G_n(s) = \frac{y(s)}{n(s)} = -\frac{k_p+G_z(s)\cdot s}{k_p+s} \end{cases} \tag{16}$$

where $G_r(s)$, $G_f(s)$, and $G_n(s)$ denote the transfer functions reflecting the tracking performance, disturbance rejection ability, and the noise suppression property, respectively.

According to (16), the disturbance rejection can be adjusted by devising $G_z(s)$ without affecting the tracking performance, and two degree-of-freedom control can be realized. Particularly, the characteristics of $G_z(s)$ will determine the disturbance rejection and noise suppression ability once the controller gain k_p is settled.

The conventional method for $G_z(s)$ follows the set as

$$\beta_1 = 4\omega_o,\ \beta_2 = 6\omega_o^2,\ \beta_3 = 4\omega_o^3,\ \beta_4 = \omega_o^4. \tag{17}$$

which simplifies the multiple parameters to the tuning of bandwidth ω_o. The tuning procedure is simple, but the influence of each parameter on observer performance is unclear.

The explicitly analytical relationship between the observer gains and performance is impossible to be obtained according to the existing theoretical results. Instead, frequency analysis method could be applied to qualitatively acquire some directive conclusions [32].

The expressions of amplitude gain of $G_f(s)$, $G_n(s)$, defined as $|G_f(j\omega)|$, $|G_n(j\omega)|$, can be deduced by (18). It is expected that smaller gain of $G_f(s)$ at low frequency will improve the accuracy of disturbance estimation and smaller gain of $G_n(s)$ at high frequency will improve the noise suppression ability.

With predefined value, $k_p = 26$, $\omega_o = 450$ rad/s, the partial derivatives of $|G_f(j\omega)|$, $|G_n(j\omega)|$ are solved. Parameters are preliminarily determined by (17). It is found that at lower frequency range, the partial derivatives of $|G_f(j\omega)|$ satisfy (19) and (20). The value of $|G_f(j\omega)|$ increases with β_1 but decreases with β_4. Therefore, smaller value of β_1 or greater value of β_4 will contribute to the enhanced disturbance estimation accuracy. Additionally, at higher frequency range, the partial derivative of $|G_n(j\omega)|$ satisfies (21). Value of $|G_n(j\omega)|$ increases with β_2. It indicates that smaller value of β_2 produces stronger noise immunity.

$$\frac{\partial |G_f(\beta_1,\beta_2,\beta_3,\beta_4)|}{\partial \beta_1} > 0 \tag{19}$$

$$\frac{\partial |G_f(\beta_1,\beta_2,\beta_3,\beta_4)|}{\partial \beta_4} < 0 \tag{20}$$

$$|G_f(j\omega)| = \left|\frac{1-G_z(s)}{k_p+s}\right| = \frac{\sqrt{(\omega^8 + \beta_1^2\omega^6)}}{\sqrt{((k_p+\beta_1)\omega^4 - (k_p\beta_2+\beta_3)\omega^2 + k_p\beta_4)^2 + (\omega^5 - (k_p\beta_1+\beta_2)\omega^3 + k_p\beta_3\omega + \beta_4\omega)^2}}$$

$$|G_n(j\omega)| = \left|-\frac{k_p+G_z(s)\cdot s}{k_p+s}\right| = \frac{\sqrt{(k_p(\omega^4 - \beta_2\omega^2 + \beta_4) - \beta_3\omega^2)^2 + (\beta_3 k_p\omega + \beta_4\omega - \beta_1 k_p\omega^3 - \beta_2\omega^3)^2}}{\sqrt{((k_p+\beta_1)\omega^4 - (k_p\beta_2+\beta_3)\omega^2 + k_p\beta_4)^2 + (\omega^5 - (k_p\beta_1+\beta_2)\omega^3 + k_p\beta_3\omega + \beta_4\omega)^2}} \tag{18}$$

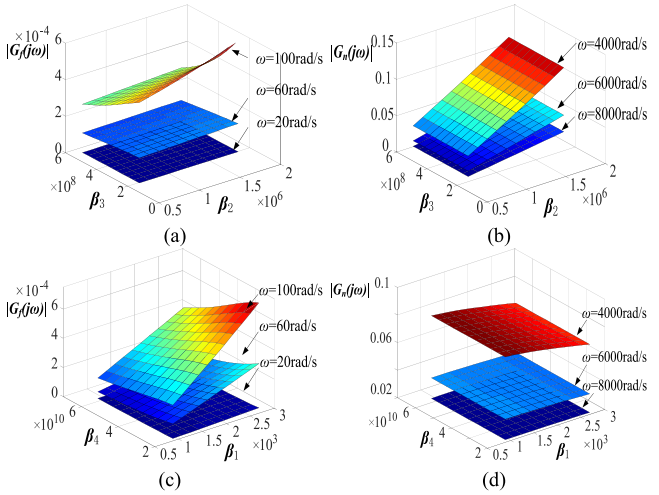

Fig. 4. $|G_f(j\omega)|$ and $|G_n(j\omega)|$ as functions of four parameters. (a) $|G_f(j\omega)|$ regarding β_2, β_3. (b) $|G_n(j\omega)|$ regarding β_2, β_3. (c) $|G_f(j\omega)|$ regarding β_1, β_4. (d) $|G_n(j\omega)|$ regarding β_1, β_4.

$$\frac{\partial\,|G_n(\beta_1,\beta_2,\beta_3,\beta_4)|}{\partial\beta_2} > 0. \tag{21}$$

Fig. 4 plots the values of $|G_f(j\omega)|$ and $|G_n(j\omega)|$ with respect to parameters in $G_z(s)$. Each parameter varies from 50% to 150% of the reference value in (17). In Fig. 4(a), the variation of β_2 and β_3 has little effects on the value of $|G_f(j\omega)|$ at the low frequency. It means that disturbance estimation accuracy is less related to the change of β_2 and β_3. In Fig. 4(b), the value of $|G_n(j\omega)|$ at high frequency increases with β_2, demonstrating that the noise immunity could be enhanced by reducing β_2. In Fig. 4(c), the value of $|G_f(j\omega)|$ increases with β_1 while decreases with β_4, which coincides with (19), (20). Meanwhile, their impact on the noise immunity is negligible as the value of $|G_n(j\omega)|$ changes a little with the variation of two parameters in Fig. 4(d).

According to above-mentioned analysis, further efforts could be made to tuning parameters in (17) to improve the performance of HESO.

As denoted by (13), the characteristic polynomial is

$$s^4 + \beta_1' s^3 + \beta_2' s^2 + \beta_3' s + \beta_4' = 0. \tag{22}$$

We design it composed of two second-order factors, as follows:

$$D(s) = (s^2 + 2\zeta\omega_o s + \omega_o^2)(s^2 + 2\alpha\zeta\omega_o s + \alpha^2\zeta^2\omega_o^2) \tag{23}$$

where ω_o is the bandwidth of observer, parameter ζ and α are selected to meet the design requirement. Equating the coefficients of (22) and (23) yields the following relationships:

$$\begin{cases} \beta_1' = 2(\alpha+1)\zeta\omega_o \\ \beta_2' = (\alpha^2\zeta^2 + 4\alpha\zeta^2 + 1)\omega_o^2 \\ \beta_3' = 2\alpha\zeta(\zeta^2+1)\omega_o^3 \\ \beta_4' = \alpha^2\zeta^2\omega_o^4. \end{cases} \tag{24}$$

As mentioned previously, β_4 has prominent impacts on the disturbance rejection performance of the observer. In our case, we set $\alpha\zeta = 1$ to retain the similar disturbance rejection property to the conventional gains. As a result, (24) is simplified as follows:

$$\begin{cases} \beta_1' = (2+2\zeta)\omega_o \\ \beta_2' = (2+4\zeta)\omega_o^2 \\ \beta_3' = 2(\zeta^2+1)\omega_o^3 \\ \beta_4' = \omega_o^4. \end{cases} \tag{25}$$

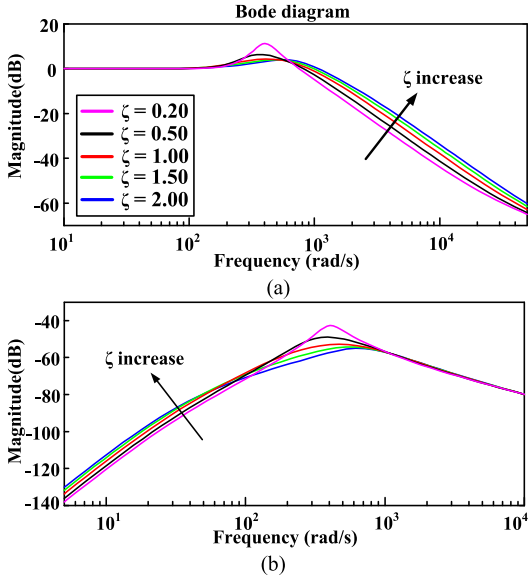

Fig. 5. Frequency characteristics of HESO with ζ variation. (a) Noise suppression function. (b) Disturbance rejection function.

It can be observed from (25) that novel gain combinations share the similar formality with those tuned by bandwidth method. Moreover, an extra parameter ζ is included in (25), which gains additional degree of freedom in designing the observer except for bandwidth ω_o.

Fig. 5 shows Bode diagram of fourth-order HESO with bandwidth $\omega_o = 450$ rad/s and ζ varying from 0.2 to 2. It can be found that as ζ decreases, the property of noise suppression of the observer is enhanced. This can be explained by the decrease of β_2 as analyzed previously. A special case is that when $\zeta = 1$, (25) is identical to the conventional gains (17), where the noise immunity is weaker. Interestingly, the disturbance rejection performance in the lower frequency range is not attenuated but improves a little with smaller ζ. That means the selection of ζ does not encounter the tradeoff between disturbance rejection and noise immunity. It should be noticed that, to avoid worse disturbance rejection property in the medium frequency, ζ cannot be set too small.

Ultimately, we fix the parameters in (24) as

$$\zeta = 0.25\ ,\ \alpha = 4 \tag{26}$$

and the new parameter set becomes

$$\beta_1' = 5\omega_o/2,\ \ \beta_2' = 3\omega_o^2,\ \ \beta_3' = 17\omega_o^3/8,\ \ \beta_4' = \omega_o^4. \tag{27}$$

From (27), it can be found that the new set retains the parameter ω_o, so it is convenient to determine the gains by trial and error in practical application, just like parameter tuning by bandwidth method.

HESO adopting the gains in (27) is defined as HESO1 and that adopting conventional gains in (17) is defined as HESO2. Fig. 6 depicts the frequency response of HESO1 and HESO2. From this figure, it can be known that magnitude of HESO1 is smaller than HESO2 with regard to noise suppression function at high frequency and disturbance rejection function at low frequency. The former has higher peak magnitude around medium frequency, while the latter has lower magnitude. The performance comparisons of two types of HESO are illustrated in Table II. It implies that HESO1 is advisable for better disturbance rejection

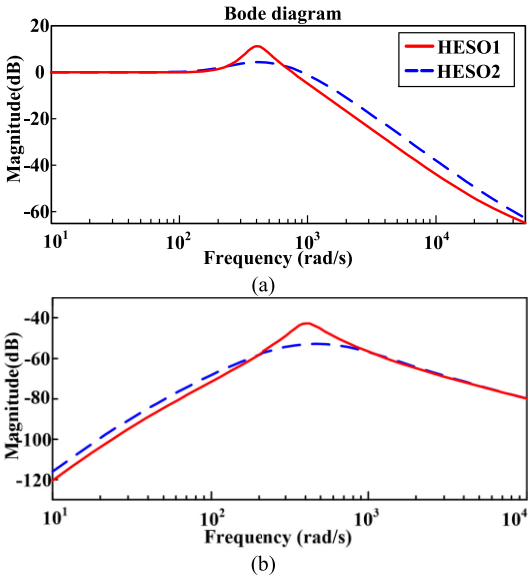

Fig. 6. Frequency characteristics of HESO1 and HESO2. (a) Noise suppression function. (b) Disturbance rejection function.

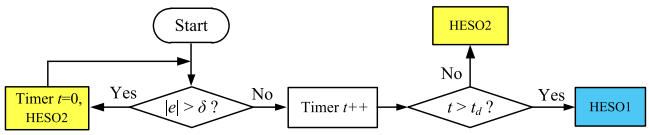

Fig. 7. Flowchart of switching logic.

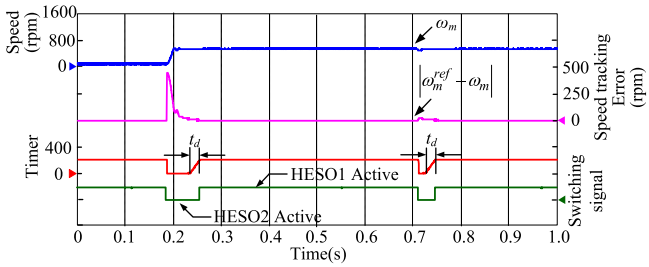

Fig. 8. Control response with switching mechanism.

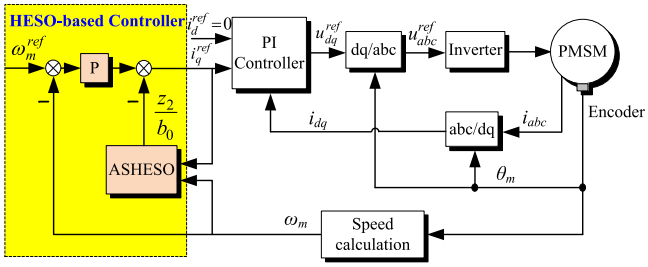

Fig. 9. Schematic diagram of PMSM drive system with ASHESO.

TABLE II
PERFORMANCE COMPARISONS OF HESO1 AND HESO2

	HESO1	HESO2
Fluctuation in transient state	great	small
Disturbance rejection performance at low frequency	higher	lower
Noise suppression performance at high frequency	higher	lower

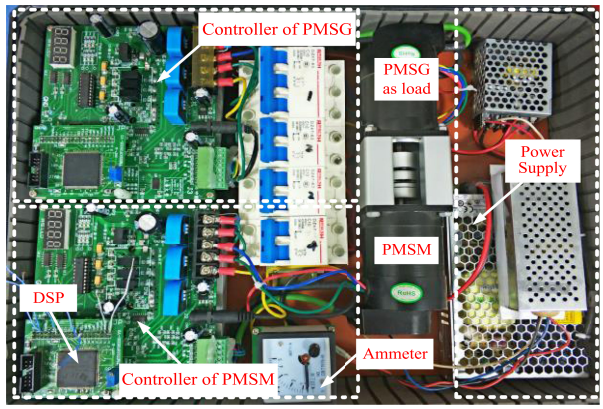

Fig. 10. Experimental platform for PMSM system.

and noise suppression performance, whereas HESO2 is applied for better dynamic response.

B. Adaptive Mechanism for ASHESO

According to the above-mentioned analysis, both HESO1 and HESO2 have their own advantages and disadvantages. It will be useful to incorporate both the merits of the observers. To realize it, an adaptive mechanism is proposed by switching over HESO1 and HESO2 according to the tracking error and setting time of estimation.

The flowchart of switching logic is depicted in Fig. 7. The scheme is explained as follows.

1) *Transient state operation*: Define the error between the reference r and output state y as symbol e. If absolute value of e is greater than the threshold value δ, HESO2 will be adopted and the delay timer is reset.
2) *Delay timer counting*: Since the dynamic response of HESO generally has overshoot and setting time, the certain delay time t_d should be included once the output state enters the convergence zone. It avoids the output state to enter steady-state range initially but overshoot out of the range again. HESO2 is still adopted at this stage.
3) *Steady-state operation*: After delay time t_d and while absolute value of e is smaller than δ, observer will switch to HESO1.

Next, we will discuss how to select the threshold value δ and delay time t_d.

1) Selection of Threshold Value δ: The threshold value δ is mainly influenced by periodic disturbance like speed ripple. For fourth-order HESO, the relationship between the steady-state error and disturbance signal is formulated as

$$G_f(s) = \frac{1 - G_z(s)}{k_p + s} = \frac{s^4 + \beta_1 s^3}{(k_p + s)(s^4 + \beta_1 s^3 + \beta_2 s^2 + \beta_3 s + \beta_4)}. \quad (28)$$

Assume that reference signal is constant in the steady state. When the system is influenced by sinusoidal disturbance and the function is known as $f = M_1 \cdot \sin(\omega t)$, the maximum output

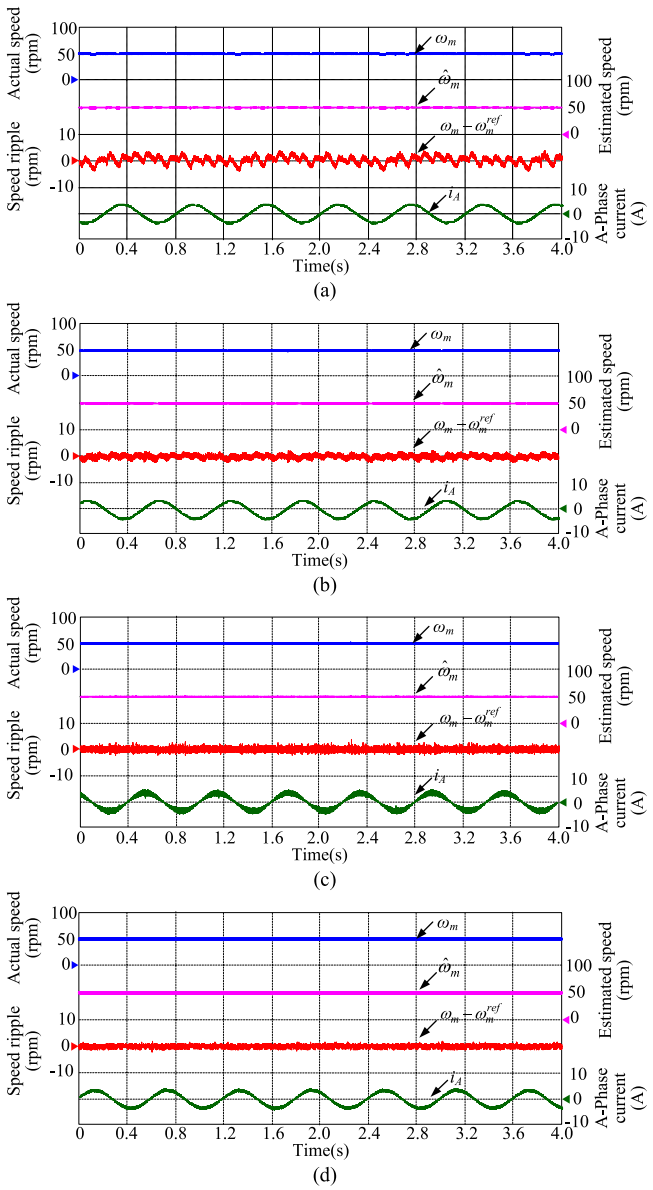

Fig. 11. Steady-state experimental results at speed of 50 r/min. (a) PI. (b) CESO. (c) HESO. (d) ASHESO.

steady-state error is derived as

$$|e|_{\max} = \frac{M_1\sqrt{\omega^8+16\omega^6\omega_o^2}}{\sqrt{k_p^2+\omega^2}\cdot\sqrt{\omega^8+\omega_o^8+6\omega^4\omega_o^4+4\omega^6\omega_o^2+4\omega^2\omega_o^6}} = \frac{M_1k^3\sqrt{k^2+16}}{(k^2+1)^2\cdot\sqrt{k_p^2+\omega^2}} \tag{29}$$

where k is the ratio of signal frequency ω to the observer bandwidth ω_o.

As the speed ripple generally contains multiple frequency components, the error at different frequencies can be calculated according to (29). Consequently, the threshold value should be set as the maximum value of steady-state error

$$\delta = \max(|e_i|_{\max}), \quad i = 1,\ 2,\ 3\ldots \tag{30}$$

where i represents the index of the frequency components involved in the disturbance signal.

If the magnitude and frequency of periodic disturbance is unknown, the threshold can be determined according to the real practice of the drive system. It is convenient to acquire the maximum tracking error in steady state by measuring the speed within the operation range. When the motor works in the transient state, the error between the output and the reference is far greater than that in the steady state and it decreases globally. It is advisable to design δ slightly larger than the actual steady-state tracking error and the amplification of dynamic error will not give rise to vibration of the speed.

2) Selection of Delay Time t_d: Delay time t_d can be obtained by either experiments or time response analysis. The setting time of HESO is associated with the disturbance and the acquisition of t_d will also depend on the disturbance formality. Step or ramp torque disturbance generally has greater impact on speed dynamic response than periodic disturbance. Therefore, theoretical calculation of t_d will take these two types of disturbance into consideration.

If the disturbance satisfies the step function as $f(s) = M_2/s$, the response of fourth-order HESO is

$$\hat{f}(s) = M_2\left(\frac{1}{s} - \frac{1}{s+\omega_o} - \frac{\omega_o}{(s+\omega_o)^2} + \frac{5\omega_o^2}{(s+\omega_o)^3} - \frac{3\omega_o^3}{(s+\omega_o)^4}\right). \tag{31}$$

The inverse Laplace transform of (31) can be obtained as

$$\hat{f}(t) = M_2 - M_2\left(1+\omega_o t - \frac{5}{2}\omega_o^2t^2 + \frac{1}{2}\omega_o^3t^3\right)e^{-\omega_o t}. \tag{32}$$

Take the derivative of (32), and let $\dot{\hat{f}}(t) = 0$, the extreme points will be

$$t_1 = 2/\omega_o, \quad t_2 = 6/\omega_o. \tag{33}$$

According to (33), there are two extreme points in the step response of fourth-order HESO and they are independent of the disturbance magnitude. Substitute (33) into (32) and there comes

$$\hat{f}(t_1) \approx 1.406M_2, \quad \hat{f}(t_2) \approx 0.938M_2. \tag{34}$$

When $t = t_2$, the estimate is about 93.8% of the actual magnitude of disturbance, close to the convergence region of 5%. Delay time t_d is expected to be slightly greater than t_2 and (35) will be an appropriate selection for step disturbance.

$$t_d = 10/\omega_o. \tag{35}$$

If the disturbance satisfies the ramp function, the setting time of HESO is influenced by the ratio of steady-state magnitude to slope of ramp function. The tracking process includes dynamic tracing and steady-state adjustment. The conservative estimate of delay time for ramp disturbance could be step response time as calculated by (35).

Fig. 8 shows the experimental results with the variation of speed reference and torque load. As shown in Fig. 8, the step change of reference causes great tracking error. HESO2 is adopted in this instance, giving the smooth and rapid dynamic response. When speed enters steady state, the delay timer keeps counting before reaching the set value t_d. While the error is smaller than δ, the observer switches to HESO1 to provide excellent disturbance rejection and noise suppression performance.

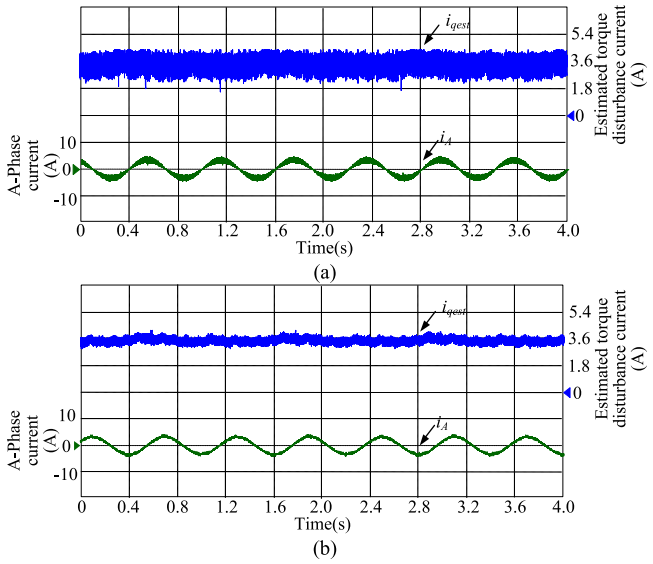

Fig. 12. Estimated torque disturbance current and phase current. (a) HESO. (b) ASHESO.

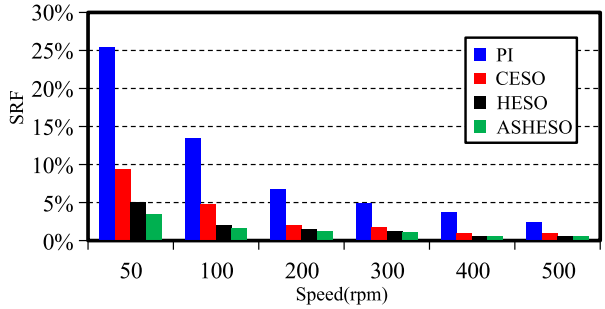

Fig. 13. SRF values of speed for different methods from 50 to 500 r/min.

The following deviation from equivalent point will reset the delay timer and cause switching action.

C. Stability Analysis

Assume that total disturbance f is bounded and varies slowly relative to observer dynamics. The assumption is generally satisfied in speed drive system.

ASHESO constructed for (4) is

$$\begin{cases} \dot{z}_1 = z_2 + \beta_1 \cdot \varphi_1 \cdot e_1 + b_0 u \\ \dot{z}_2 = z_3 + \beta_2 \cdot \varphi_2 \cdot e_1 \\ \dot{z}_3 = z_4 + \beta_3 \cdot \varphi_3 \cdot e_1 \\ \dot{z}_4 = \beta_4 \cdot \varphi_4 \cdot e_1 \\ e_1 = y - z_1 \end{cases} \tag{36}$$

where ϕ_i is ratio of gain of HESO1 to gain of HESO2 and the expression is denoted as

$$\varphi_i = \begin{cases} k_{\beta i}, & |e| \le \delta \\ 1, & |e| > \delta \end{cases}, \quad i = 1, 2, 3, 4. \tag{37}$$

Define $\varepsilon = \omega_m^{ref} - \omega_m$, $e_1 = y - z_1$, $e_2 = f - z_2$, $e_3 = \dot{f} - z_3$, $e_4 = \ddot{f} - z_4$. Combining (4) and (36), the estimation error dynamics can be deduced as

$$\dot{e} = A_4 e + b_1 f^{(3)} \tag{38}$$

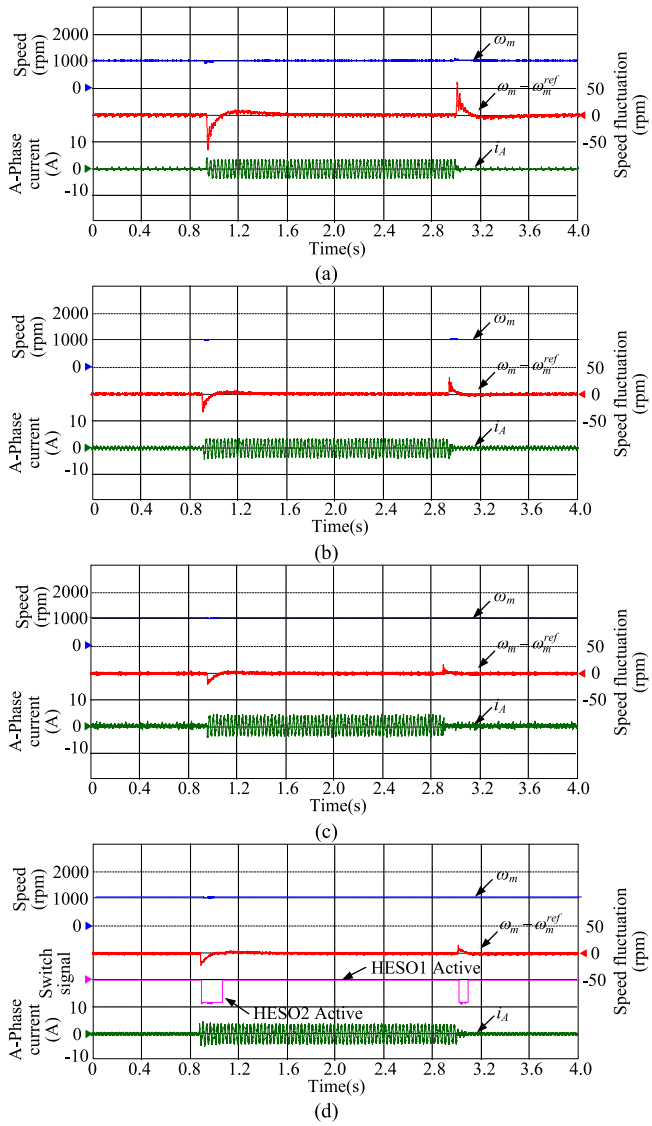

Fig. 14. Dynamic experimental results with step load torque. (a) PI. (b) CESO. (c) HESO. (d) ASHESO.

where $e = [e_1\ e_2\ e_3\ e_4]^T$, $A_4 = \begin{bmatrix} -\beta_1\varphi_1 & 1 & 0 & 0 \\ -\beta_2\varphi_2 & 0 & 1 & 0 \\ -\beta_3\varphi_3 & 0 & 0 & 1 \\ -\beta_4\varphi_4 & 0 & 0 & 0 \end{bmatrix}$,

$b_1 = [0\ 0\ 0\ 1]^T$.

Combining (12) and (36), the closed loop control error is

$$\dot{\varepsilon} = -k_p \varepsilon - B_4 e \tag{39}$$

where $B_4 = [0\ -1\ 0\ 0]$.

Combining (38) and (39), the dynamic of closed loop system can be obtained as

$$\begin{bmatrix} \dot{\varepsilon} \\ \dot{e} \end{bmatrix} = \begin{bmatrix} -k_p & B_4 \\ \mathbf{0} & A_4 \end{bmatrix} \begin{bmatrix} \varepsilon \\ e \end{bmatrix} + b_2 f^{(3)} \tag{40}$$

where $b_2 = [0\ 0\ 0\ 0\ 1]^T$.

It has been proved that $\boldsymbol{A_4}$ is Hurwitz matrix as switching gain φ_i keeps the eigenvalue of $\boldsymbol{A_4}$ placed in the left half-plane. Likewise, $\begin{bmatrix} -k_p & B_4 \\ \mathbf{0} & A_4 \end{bmatrix}$ is Hurwitz matrix as well. Therefore, the closed-loop system is asymptotically stable.

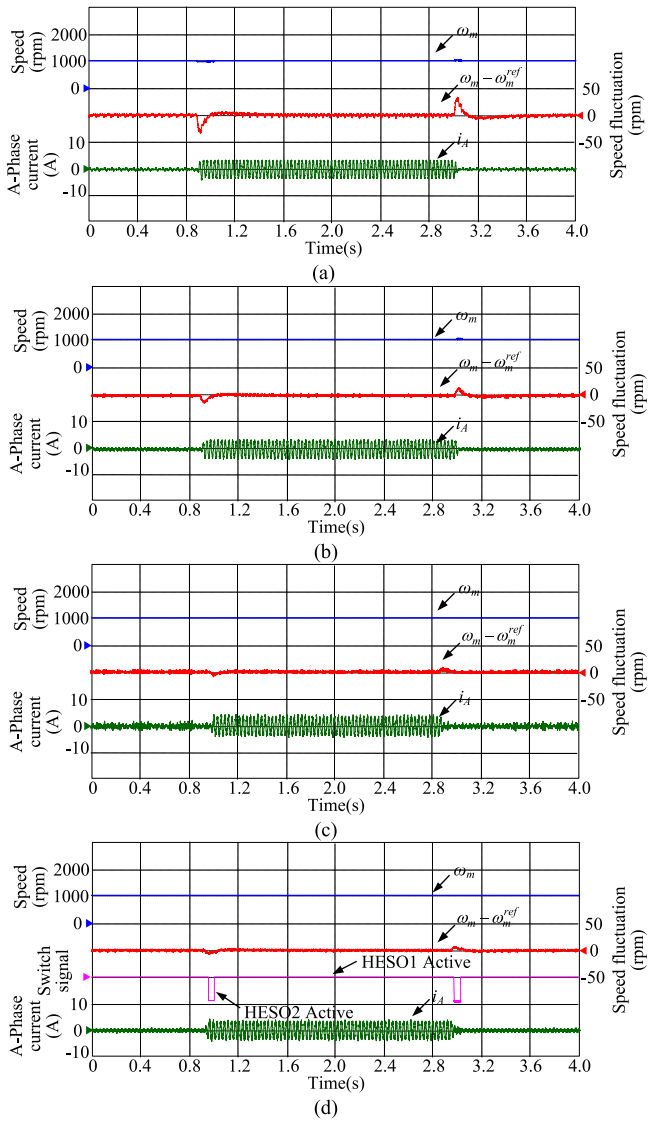

Fig. 15. Dynamic experimental results with ramp load torque. (a) PI. (b) CESO. (c) HESO. (d) ASHESO.

IV. Experimental Results and Analysis

In this section, to verify the performance of the proposed scheme, some experiments are performed on a laboratory PMSM drive system. PI control, ADRC schemes based on conventional ESO (CESO), HESO and ASHESO are implemented on the controller, respectively. The schematic diagram of PMSM drive system with ASHESO is shown in Fig. 9. The experimental platform is shown in Fig. 10. It is mainly composed of digital signal processor TMS320F28335 and three-phase inverter. The bus voltage is 24 V and the PWM frequency is 100 μs. The phase current is measured by Hall sensor and the rotor position is measured by incremental encoder. The control period of speed loop and current loop are designed as 500 and 100 μs severally. The parameters of PMSM are summarized in Table III. In Fig. 10, PMSM is the controlled motor for algorithm verification and PMSG is used for applying load torque.

Due to the influence of sensor measurement error, inverter nonlinearity and motor shaft misalignment, there are multiple frequency speed ripples when the motor works at low speed. To fairly evaluate the control performance of the algorithm, parameters of the controller in four methods are chosen to make the system to have the similar bandwidth. The bandwidth of speed control adopting PI controller are determined according to the formula: $K_{\rm sp} = \omega_{\rm sc} K_t/J$, $K_{\rm si} = \omega_{\rm sc} K_{\rm sp}/h$, where $\omega_{\rm sc}$ represents the cutoff pulsation of the speed loop, which is set as 63 rad/s. h is referred as the damping coefficient and the value is 5 rad. The bandwidth ω_o of the observer is set as 450 rad/s. The feedback gain of ADRC schemes is $k_p = 63\ {\rm s}^{-1}$. The threshold for convergence region is set as $\delta = 4.5$ r/min and delay time is calculated as $t_d = 0.022$ s.

TABLE III
Main Parameters of PMSM System

Parameter	Value
Rated power/W	60
Rated speed/rpm	3000
Rated torque/N.m	0.2
Stator resistance/ Ω	0.31
Pole pairs	2
D-axes inductance/mH	2.5
Q-axes inductance/mH	2.6
Magnet flux linkage/Wb	0.01428
Rated voltage/VDC	24
Rated current/A	4.6
Moment of inertia/kg.cm^2	4.808

TABLE IV
Summary of Dynamic Experimental Results

Strategy	Speed fluctuation/ rpm		Recovery time/ s	
	Step load	Ramp load	Step load	Ramp load
PI	57	41	0.120	0.160
ESO	20	15	0.102	0.128
HESO/ ASHESO	8	5	0.076	0.094

A. Steady-State Experimental Study

To evaluate the steady-state performance of four methods, the experiments at different speed are performed. The steady-state results of output speed at 50 r/min under the rated load are depicted in Fig. 11.

The waveforms of speed, estimated speed, speed ripple, and phase current are plotted, respectively. It can be seen from Fig. 11(a) that PI control cannot suppress the torque ripple efficiently, resulting in large speed ripple at low speed. The maximum amplitude of ripple is around 6 r/min. When using conventional ESO, as shown in Fig. 11(b), the speed ripple is suppressed, and the amplitude is reduced to less than 3 r/min. According to Fig. 11(c), the speed is more sensitive to measurement noise with HESO algorithm. Hence, the smoothness of speed is worsened. When ASHESO is executed, as depicted in Fig. 11(d), the sensitivity of output speed to noise is reduced and the ripple amplitude is diminished to 1 r/min.

Fig. 12 compares the estimated torque disturbance current obtained by HESO and ASHESO. As shown in Fig. 12(a), due to the poor noise immunity property of HESO, more significant noise amplification occurs in the estimated current. Even if

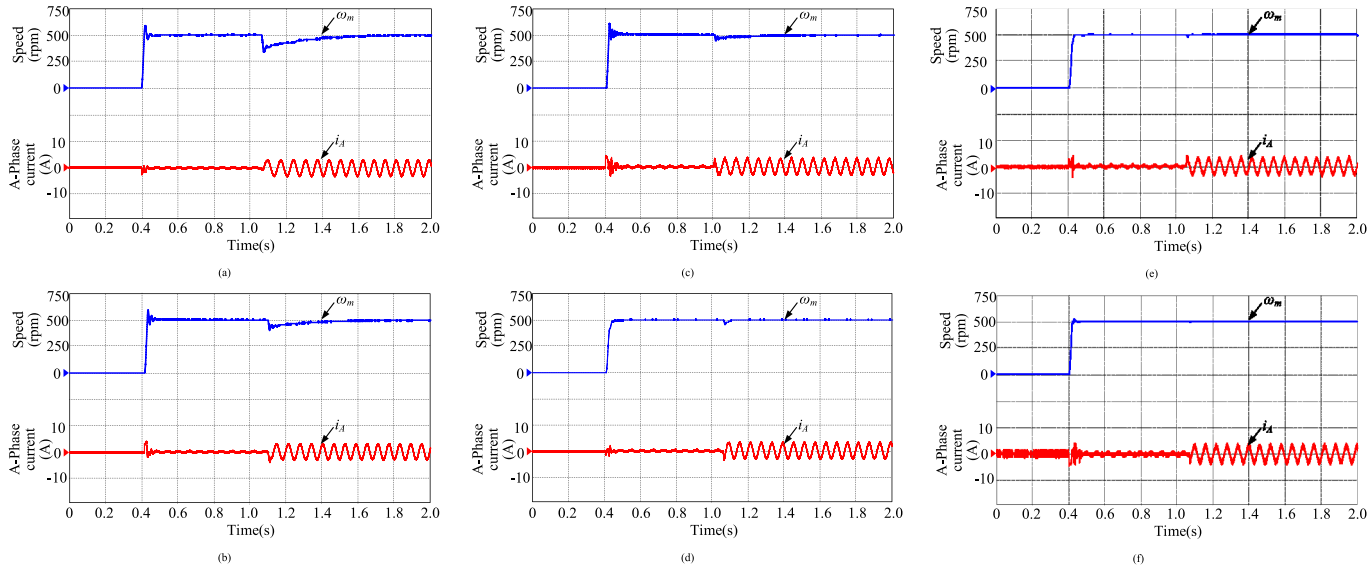

Fig. 16. Robustness study with mismatch of the moment of inertia. (a) PI, J = 0.5Jn. (b) PI, J = Jn. (c) PI, J = 2Jn. (d) ASHESO, J = 0.5Jn. (e) ASHESO, J = Jn. (f) ASHESO, J = 2Jn.

TABLE V
PERFORMANCE COMPARISONS OF PI, CESO, HESO, AND ASHESO

	PI	CESO	HESO	ASHESO
Fluctuation in transient state	great	great	small	small
Convergence rate of estimation error		slow	fast	fast
Disturbance rejection precision at low frequency	lower	lower	medium	higher
Noise suppression performance at high frequency	higher	higher	lower	medium

the bandwidth is increased, the improvement effect of speed control accuracy will not be obvious. Nevertheless, ASHESO acquires superior noise suppression characteristics. The noise is constrained to desired level in estimated signal. Hence, it is possible for ASHESO to obtain better control performance.

Steady-state results under other speed are evaluated by speed ripple factor (SRF), as illustrated by (41), which is defined as a criterion of speed ripple reduction. It is assessed as the percentage of deviation from the reference value, where $\omega_{m\_pk\text{-}pk}$ is the peak-to-peak speed ripples

$$SRF = \frac{\omega_{m\_pk-pk}}{\omega_m^{ref}} 100(\%). \tag{41}$$

Fig. 13 plots SRF value of steady-state speed with rated load when the motor operates at the speed from 50 to 500 r/min. It can be seen that when the speed increases, the speed ripple generally reduces. Compared with PI control, the speed ripple with ESO-based schemes decreases to less than one half of the level achieved by the former. It proves that ESO-based schemes acquire periodic disturbance rejection ability to some extent. Particularly, thanks to the higher estimation accuracy and superior noise suppression property, ASHESO achieves the minimum speed ripple among the methods to be compared.

B. Dynamic State Experimental Study

In order to analyze the disturbance rejection performance of four methods, experiments with the sudden change of load torque when the machine works at 1000 r/min have been operated. The load torque is applied by the step and ramp formalities. Figs. 14 and 15 describe the dynamic waveforms with abrupt step and ramp load. The experimental results including speed fluctuation and recovery time are detailed in Table IV. It can be seen from Fig. 14 that speed fluctuations under PI control, CESO, HESO, and ASHESO schemes are 57 r/min, 20 r/min, and 8 r/min, respectively, which illustrates that HESO and ASHESO perform best for step disturbance rejection. Benefited from the rapid estimation rate of disturbance, it takes shorter recovery time for speed to return back to the set value when HESO or ASHESO is adopted. Therefore, speed control based on HESO-type algorithm achieves optimal dynamic performance when step load is applied. The results and conclusions are also applicable with regard to ramp torque disturbance.

Figs. 14(d) and 15(d) show that ASHESO adopts HESO2 during transient process, the speed tracking rate under ASHESO is swift and speed fluctuation is small. Since HESO2 shares the identical gain with HESO, the dynamic performance of ASHESO is comparable to HESO. Once the speed enters the steady state, ASHESO switches to HESO1 with another set of

gain. The noise is reduced to desired level in the speed and current signal. And the noise immunity and estimation accuracy of ASHESO are improved.

C. Robustness Study for Parameter Variation

Apart from different types of external disturbance, internal uncertainties like parameter variation are generally existent in electrical drive systems. In order to analyze the robustness of proposed scheme for parameter variation, a series of comparative experiments under inertia mismatch are implemented. Suppose that the knowledge of system inertia is not precise, the controller is designed with different inertia, but tested in the same platform. Fig. 16 shows speed tracking response when startup and step loading. The estimate of inertia varies from 50% to 200% of actual value. For comparison, speed tracking test under PI control is also conducted.

It is shown from the results that when the moment of inertia mismatches, the performance of speed control based on PI controller is more seriously affected. Specifically, if the inertia is underestimated, as plotted in Fig. 16(a), speed overshoot is diminished but the speed drop becomes greater and it takes longer recovery time. If the inertia is overestimated, as shown in Fig. 16(c), speed overshoot during the startup is more obvious and the speed fluctuation is reduced when step load torque is exerted. By contrast, speed tracking performance with ASHESO scheme is less affected by inertia mismatch. It is demonstrated in Fig. 16(d), (e), and (f) that inertia mismatch within a certain range does not produce overshoot during startup. The influence on load torque disturbance rejection performance is also minor compare to PI control.

In brief, the conclusions obtained from the theoretical comparison and experimental results on the performance of the methods assessed in this article are tabulated in Table V.

V. Conclusion

This article proposed an enhanced speed controller for electrical drives based on ASHESO. First, the proposed observer adopts new gain method, which modifies a part of pole locations of observer. Analytical results illustrate that the proposed gain has benefit of improving the robustness to measurement noise without attenuating the disturbance rejection ability. Moreover, in case of transient state with abrupt disturbance, an adaptive switching mechanism based on tracking error is proposed in this article, which ensures that the observer achieves both rapid tracking response and excellent steady-state performance.

Strategies including PI control, conventional ESO, HESO, and ASHESO are compared on a laboratory PMSM drive system. The results demonstrate that ASHESO has better disturbance rejection performance than PI control and the conventional ESO. Compared with HESO utilizing the traditional gain, ASHESO is less sensitive to measurement noise and achieves better suppression on speed ripple. Besides, ASHESO can reduce the speed fluctuation to the greatest extent when sudden load torque is applied. The robustness of ASHESO to parameter variation is also verified by a series of test.

The proposed speed controller can also be readily extended to other systems such as induction motor drive.

References

[1] P. Pillay and R. Krishnan, "Control characteristics and speed controller design for a high performance permanent magnet synchronous motor drive," *IEEE Trans. Power Electron.*, vol. 5, no. 2, pp. 151–159, Apr. 1990.

[2] C.-M. Liaw and C.-M. Wu, "Design and implementation of a high-performance field-oriented induction motor drive," *IEEE Trans. Ind. Electron.*, vol. 38, no. 4, pp. 275–282, Aug. 1991.

[3] R. Sanchis, J. A. Romero, and P. Balaguer, "A simple procedure to design PID controllers in the frequency domain," in *Proc. 35th Annu. Conf. IEEE Ind. Electron. Soc.*, Nov. 2009, pp. 1420–1425.

[4] J. Holtz and L. Springob, "Identification and compensation of torque ripple in high-precision permanent magnet motor drives," *IEEE Trans. Ind. Electron.*, vol. 43, no. 2, pp. 309–320, Apr. 1996.

[5] C. De Angelo, G. Bossio, J. Solsona, G. O. Garcia, and M. I. Valla, "Mechanical sensorless speed control of permanent-magnet AC motors driving an unknown load," *IEEE Trans. Ind. Electron.*, vol. 53, no. 2, pp. 406–414, Apr. 2006.

[6] L. Harnefors, S. E. Saarakkala, and M. Hinkkanen, "Speed control of electrical drives using classical control methods," *IEEE Trans. Ind. Appl.*, vol. 49, no. 2, pp. 889–898, Mar./Apr. 2013.

[7] W. Qian, S. K. Panda, and J. X. Xu, "Speed ripple minimization in PM synchronous motor using iterative learning control," *IEEE Trans. Energy Convers.*, vol. 20, no. 1, pp. 53–61, Mar. 2005.

[8] S. Hara, Y. Yamamoto, T. Omata, and M. Nakano, "Repetitive control system: A new type servo system for periodic exogenous signals," *IEEE Trans. Autom. Control*, vol. 33, no. 7, pp. 659–668, Jul. 1988.

[9] P. Mattavelli, L. Tubiana, and M. Zigliotto, "Torque-ripple reduction in PM synchronous motor drives using repetitive current control," *IEEE Trans. Power Electron.*, vol. 20, no. 6, pp. 1423–1431, Nov. 2005.

[10] Z. Zhou, C. Xia, Y. Yan, Z. Wang, and T. Shi, "Disturbances attenuation of permanent magnet synchronous motor drives using cascaded predictive-integral-resonant controllers," *IEEE Trans. Power Electron.*, vol. 33, no. 2, pp. 1514–1527, Feb. 2018.

[11] K. Ohnishi, "A new servo method in mechatronics," *Trans. Jpn. Soc. Elect. Eng.*, vol. 107, pp. 83–86, 1987.

[12] C. Johnson, "Accommodation of external disturbances in linear regulator and servomechanism problems," *IEEE Trans. Autom. Control.*, vol. 16, no. 6, pp. 635–644, Dec. 1971.

[13] Q.-C. Zhong, A. Kuperman, and R.-K. Stobart, "Design of UDE based controllers from their two-degree-of-freedom nature," *Int. J. Robust Nonlinear Control*, vol. 17, no. 21, pp. 1994–2008, 2011.

[14] S. Ye and X. Yao, "An enhanced SMO-based permanent-magnet synchronous machine (PMSM) sensorless drive scheme with current measurement error compensation," *IEEE J. Emerg. Sel. Topics Power Electron.*, vol. 9, no. 4, pp. 4407–4419, Aug. 2021, doi: 10.1109/JESTPE.2020.3038859.

[15] J. Han, "The extended state observer of a class of uncertain systems," *Control Decis.*, vol. 10, no. 1, pp. 85–88, 1995.

[16] J. Han, "From PID to active disturbance rejection control," *IEEE Trans. Ind. Electron.*, vol. 56, no. 3, pp. 900–906, Mar. 2009.

[17] S. Li and Z. Liu, "Adaptive speed control for permanent-magnet synchronous motor system with variations of load inertia," *IEEE Trans. Ind. Electron.*, vol. 56, no. 8, pp. 3050–3059, Aug. 2009.

[18] Y. Zuo, X. Zhu, L. Quan, C. Zhang, Y. Du, and Z. Xiang, "Active disturbance rejection controller for speed control of electrical drives using phase-locking loop observer," *IEEE Trans. Ind. Electron.*, vol. 66, no. 3, pp. 1748–1759, Mar. 2019.

[19] L. Qu, W. Qiao, and L. Qu, "Active-disturbance-rejection-based sliding-mode current control for permanent-magnet synchronous motors," *IEEE Trans. Power Electron.*, vol. 36, no. 1, pp. 751–760, Jan. 2021.

[20] C. Du, Z. Yin, Y. Zhang, J. Liu, X. Sun, and Y. Zhong, "Research on active disturbance rejection control with parameter autotune mechanism for induction motors based on adaptive particle swarm optimization algorithm with dynamic inertia weight," *IEEE Trans. Power Electron.*, vol. 34, no. 3, pp. 2841–2855, Mar. 2019.

[21] G. Wang, R. Liu, N. Zhao, D. Ding, and D. Xu, "Enhanced linear ADRC strategy for HF pulse voltage signal injection-based sensorless IPMSM drives," *IEEE Trans. Power Electron.*, vol. 34, no. 1, pp. 514–525, Jan. 2019.

[22] C. Liu, G. Luo, Z. Chen, and W. Tu, "Finite-time convergent multiple disturbance rejection control for electromechanical actuators," *IEEE Trans. Power Electron.*, vol. 36, no. 6, pp. 6863–6878, Jun. 2021.

[23] R. Miklosovic, A. Radke, and Z. Gao, "Discrete implementation and generalization of the extended state observer," in *Proc. Amer. Control Conf.*, Jun. 2006, pp. 2209–2214.

[24] Y. Yan, Z. Sun, and S. Li, "Disturbance rejection control method based on composite disturbance observer for permanent magnet synchronous motor," in *Proc 41st Annu. Conf. IEEE Ind. Electron. Soc.*, 2015, pp. 3137–3142.
[25] M. R. Stanković, R. Madonski, S. Shao, and D. Mikluc, "On dealing with harmonic uncertainties in the class of active disturbance rejection controllers," *Int. J. Control*, to be published, doi: 10.1080/00207179.2020.1736639.
[26] A. A. Godbole, J. P. Kolhe, and S. E. Talole, "Performance analysis of generalized extended state observer in tackling sinusoidal disturbances," *IEEE Trans. Autom. Control*, vol. 21, no. 6, pp. 2212–2223, Nov. 2013.
[27] Z. Gao, "Scaling and bandwidth-parameterization based controller tuning," in *Proc. Amer. Control Conf.*, 2003, pp. 4989–4996.
[28] R. Madonski and P. Herman, "Method of sensor noise attenuation in high-gain observers - experimental verification on two laboratory systems," In *Proc. IEEE Int. Symp. Robot. Sensors Environ.*, 2012. pp. 121–16.
[29] W. Xue, W. Bai, S. Yang, K. Song, Y. Huang, and H. Xie, "ADRC with adaptive extended state observer and its application to air–fuel ratio control in gasoline engines," *IEEE Trans. Ind. Electron.*, vol. 62, no. 9, pp. 5847–5857, Sep. 2015.
[30] K. Łakomy and R. Madonski, "Cascade extended state observer for active disturbance rejection control applications under measurement noise," *ISA Trans.,* vol. 109, pp. 1–10, 2021.
[31] R. C. Dorf and R. H. Bishop, *Modern Control Systems*. London, U. K.: Pearson, 2017, pp. 298–299.
[32] E. Sariyildiz and K. Ohnishi, "Stability and robustness of disturbance-observer-based motion control systems," *IEEE Trans. Ind. Electron.*, vol. 62, no. 1, pp. 414–422, Jan. 2015.

Shanfeng Zhu was born in Yancheng, China, in 1995. He received the B.S. degree in electrical engineering in 2017 from the Nanjing University of Aeronautics and Astronautics, Nanjing, China, where he is currently working toward the Ph.D. degree in electrical engineering.

His main research interests include advanced control theories and applications on motor drive system.

Wenxin Huang (Member, IEEE) was born in Dongtai, China, in 1966. He received the B.S. degree in microelectronics from Southeast University, Nanjing, China, in 1988, and the master's and Ph.D. degrees in electrical engineering from the Nanjing University of Aeronautics and Astronautics, Nanjing, China, in 1994 and 2002, respectively.

In 2003, he was with the Faculty of the College of Automation Engineering, Nanjing University of Aeronautics and Astronautics, where he is currently a Professor. His research interests include stand-alone power systems, power electronics, design, and control for electrical machine systems.

Yajun Zhao was born in Zhenjiang, China, in 1990. He received the B.S. and master's degrees in electrical engineering in 2012 and 2015, respectively, from the Nanjing University of Aeronautics and Astronautics, Nanjing, China, where he is currently working toward the Ph.D. degree in electrical engineering.

His current research interests include power electronics and power conversion.

Xiaogang Lin (Member, IEEE) was born in Quanzhou, China, in 1990. He received the B.S. degree from Dalian Maritime University, Dalian, China, in 2012, and the master's degree from Fuzhou University, Fuzhou, China, in 2016, and the Ph.D. degree from the Nanjing University of Aeronautics and Astronautics, Nanjing, China, in 2020, all in electrical engineering.

His current research interests include motor drive system.

Dingfeng Dong was born in Lianyungang, China, in 1982. He received the B.S. degree in electrical engineering from Nantong University, Nantong, China, in 2005, and the master's degree from Jiangsu University, Zhenjiang, China, in 2008, and the Ph.D. degree in electrical engineering from the Nanjing University of Aeronautics and Astronautics, Nanjing, China, in 2019.

His main research interests include motor design.

Wen Jiang was born in Lianyungang, China, in 1991. He received the B.S. degree in electrical engineering in 2014 from the Nanjing University of Aeronautics and Astronautics, Nanjing, China, where he is currently working toward the Ph.D. degree in electrical engineering.

His current research interests include motor design and control.

Yong Zhao was born in Zhenjiang, China, in 1991. He received the B.S. degree in automation from the Nanjing Institute of Technology, Nanjing, China, in 2014, and the master's and Ph.D. degrees in electrical engineering from the Nanjing University of Aeronautics and Astronautics, Nanjing, China, in 2017 and 2021, respectively.

His current research interests include motor design and control.

Xu Wu was born in Yancheng, China, in 1992. He received the B.S. and master's degrees from the Nanjing University of Posts and Telecommunications, Nanjing, China, in 2015 and 2018, respectively. He is currently working toward the Ph.D. degree in electrical engineering with the Nanjing University of Aeronautics and Astronautics, Nanjing, China.

His main research interests include advanced control strategies for induction motors.